Electronic Supplementary Material (ESI) for Physical Chemistry Chemical Physics.


## 1. Small Angle X-ray Scattering

Small angle X-ray scattering was performed using a Bruker D8 Discover equipped with a temperature controlled, bored graphite rod furnace, custom built at the University of York. The radiation used was copper Kα (λ = 0.154056 nm) from a 1 µS microfocus source. Diffraction patterns were recorded on a 2048x2048 pixel Bruker VANTEC 500 area detector set at a distance of 121 mm from the sample. Samples were filled into 1mm capillary tubes and aligned with a pair of 1T magnets, with the field strength at the sample position being approximately 0.6T Diffraction patterns were collected as a function of temperature and the data processed using Matlab as follows. Two-dimensional scattering patterns were collected on cooling from the isotropic liquid until crystallisation in ~ 1.2 °C intervals with a temperature accuracy of +/- 0.1 °C. The 2D SAXS pattern from an empty capillary was used as a background; this was subtracted from each frame prior to the integration step.

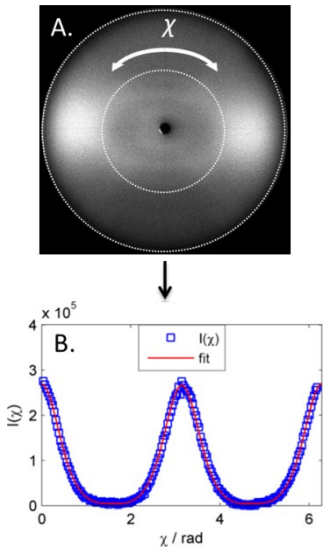


**Fig. SI-1:** (A) Background subtracted 2D SAXS pattern of RM734 at 139.8 °C; azimuthal integration gave the data shown in (B), fitting with Equation (1) allows the orientational order parameters $\langle P_n \rangle$ from the coefficients used in the fitting process ( $f_{2n}$) *via* Equations (2 – 13).

## 2. Orientational Order Parameters

2D SAXS patterns were azimuthally averaged (1 ° step size) to give scattered intensity as a function of χ for each frame (see Figure SI-1). Orientational order parameters were calculated as described elsewhere; [1-4] briefly, fitting the integrated intensity with equation (1) gives the coefficients $f_{2n}$, these are then used to determine $\langle cos^n \beta \rangle$ *via* Equations 2-6. From the values of $\langle cos^n \beta \rangle$ the orientational order parameters $\langle P_n \rangle$ can be calculated from Equations 5-11. The orientational

distribution function, $f(\beta)$, can be obtained from Equation (12) or equation (13) and is normalised against Equation (14).

$$I(X) = \sum_{0}^{\infty} \frac{\pi}{2} f_{2n} \frac{(2n-1)!!}{2^n n!} cos^{2n} X \tag{1}$$

$$\langle cos^2\beta \rangle = \sum_{n=0}^{\infty} \frac{f_{2n}}{2n+3} \Big/ \sum_{n=0}^{\infty} \frac{f_{2n}}{2n+1} \tag{2}$$

$$\langle cos^4\beta \rangle = \sum_{n=0}^{\infty} \frac{f_{2n}}{2n+5} \Big/ \sum_{n=0}^{\infty} \frac{f_{2n}}{2n+1} \tag{3}$$

$$\langle cos^6\beta \rangle = \sum_{n=0}^{\infty} \frac{f_{2n}}{2n+7} \Big/ \sum_{n=0}^{\infty} \frac{f_{2n}}{2n+1} \tag{4}$$

$$\langle cos^8\beta \rangle = \sum_{n=0}^{\infty} \frac{f_{2n}}{2n+9} \Big/ \sum_{n=0}^{\infty} \frac{f_{2n}}{2n+1} \tag{5}$$

$$\langle cos^{10}\beta \rangle = \sum_{n=0}^{\infty} \frac{f_{2n}}{2n+11} \Big/ \sum_{n=0}^{\infty} \frac{f_{2n}}{2n+1} \tag{6}$$

$$\langle P_2 \rangle = \frac{1}{2}(3\langle cos^2\beta \rangle - 1) \tag{7}$$

$$\langle P_4 \rangle = \frac{1}{8}(35\langle cos^4\beta \rangle - 30\langle cos^2\beta \rangle + 3) \tag{8}$$

$$\langle P_6 \rangle = \frac{1}{16}(231\langle cos^6\beta \rangle - 315\langle cos^4\beta \rangle - 105\langle cos^2\beta \rangle - 5) \tag{9}$$

$$\langle P_8 \rangle = \frac{1}{128}(6435\langle cos^8\beta \rangle - 12012\langle cos^6\beta \rangle + 6930\langle cos^4\beta \rangle - 1260\langle cos^2\beta \rangle + 35) \tag{10}$$

$$\langle P_{10} \rangle = \frac{1}{256}\begin{pmatrix} 46189\langle cos^{10}\beta \rangle - 109395\langle cos^8\beta \rangle \\ + 90090\langle cos^6\beta \rangle - 30030\langle cos^4\beta \rangle + 3465\langle cos^2\beta \rangle - 63 \end{pmatrix} \tag{11}$$

$$f(\beta) = \sum_{n=0}^{\infty} \frac{1+4n}{2} \langle P_{2n} \rangle P_{2n}(cos\beta) \tag{12}$$

$$f(\beta) = \sum_{n=0}^{\infty} f_{2n} cos^{2n}\beta \tag{13}$$

$$\int_{0}^{\pi} f(\beta) sin\beta d\beta = 1 \tag{14}$$

## 3. Supplementary Figures

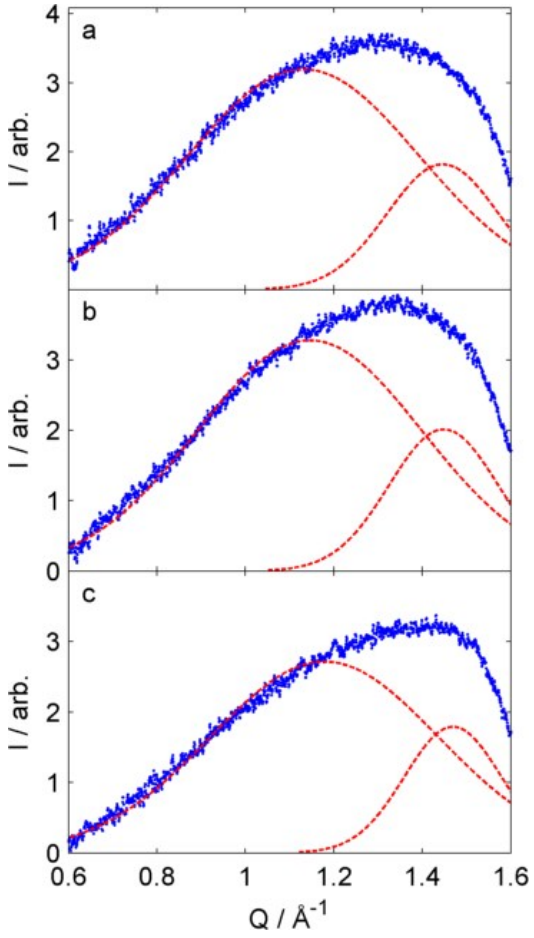


**Fig. SI-2**: Plots of wide-angle intensity (arb.) versus Q (Å$^{-1}$) for RM734 in the isotropic liquid at 190 °C (a), the nematic phase at 150 °C (b), the $N_S$ phase at 112 °C (c). Dashed lines correspond to deconvoluted peaks

## 4. Supplementary SAXS/WAXS Data

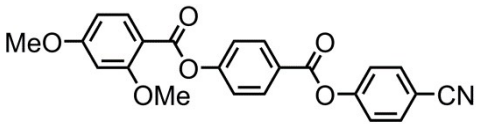


Cr 173.2 N 200.4 Iso

**RM734-CN**

**Fig. SI-3:** The molecular structure and transition temperatures of RM734-CN. [5]

As discussed in the manuscript, the splay-nematic phase has (to date) only been observed for nitro-terminated materials, with the analogous nitriles exhibiting a conventional nematic phase over wide temperature ranges. We subjected one of these materials (RM734-CN, Figure SI-3) to the same SAXS/WAXS study used on the splay-nematic material RM734 in this work.

Firstly, we observe that the behaviour of the first four even $\langle P_n \rangle$ order parameters is typical for a nematic phase, and lack the discontinuous increase seen for the splay-nematic material. The maximum value of each $\langle P_n \rangle$ of RM734-CN is roughly equal to the maximum value in the nematic phase of RM734, however values are lower than those in the splay nematic phase. At a given reduced temperature values of $\langle P_2 \rangle$, $\langle P_4 \rangle$ and $\langle P_6 \rangle$ are lower for the RM734-CN than in the nitro-terminated RM734 whereas $\langle P_8 \rangle$ was found to be fractionally larger, see Fig. SI-5. While the orientational order parameters are temperature dependent, it should also be noted that the temperature range of the nematic phase of the cyano-terminated material is larger ($\Delta T/T_{N\text{-}Iso} \approx 0.16$) than that of RM734 ($\Delta T/T_{N\text{-}Iso} \approx 0.13$). The orientational distribution function of the nitrile terminated material RM734-CN is typical and nematic like, and even at the lowest reduced temperature studied its FWHM is significantly larger than that of the splay-nematic phase of RM734. A plot $\langle P_4 \rangle$ versus $\langle P_2 \rangle$ removes the explicit temperature dependence of these two principal order parameters and shows that the behaviour of the nitro- and cyano-terminated materials is effectively identical in the nematic phase. However, the increase in both $\langle P_2 \rangle$ and $\langle P_4 \rangle$ that accompanies the onset of the $N_S$ phase is not observed for RM734-CN.

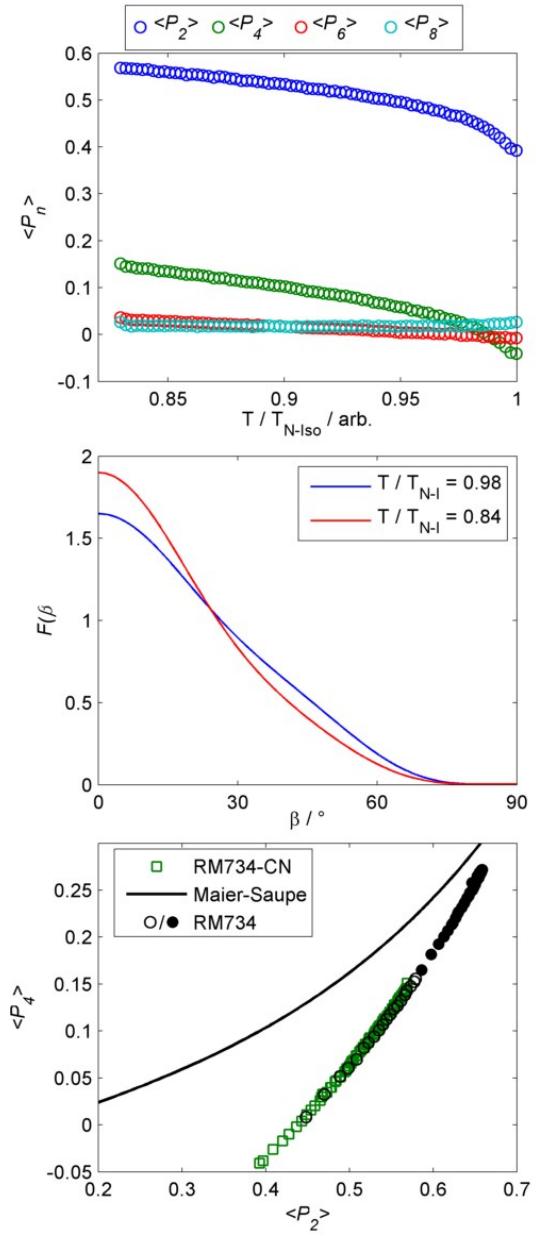


**Fig. SI-4**: Top: Plot of the first four even $\langle P_n \rangle$ order parameters of RM734-CN as a function of reduced temperature, measured as described in the manuscript text. Middle: Plot of the ODF of RM734-CN at two reduced temperatures. Bottom: Plot of $\langle P_4 \rangle$ versus $\langle P_4 \rangle$ for RM734-CN (green squares) and RM734 (empty circles = N phase, filled circles = $N_S$ phase) along with values from Maier-Saupe theory (solid line).

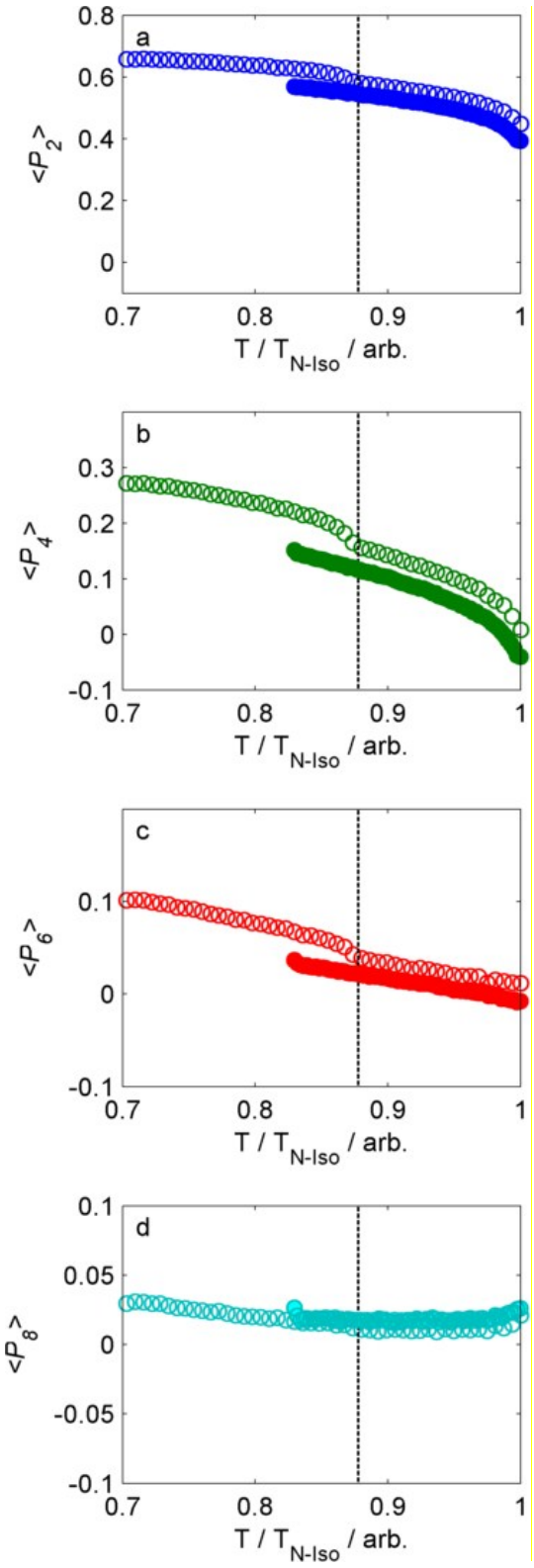


**Fig. SI-5:** Plots of the orientational order parameters $\langle P_2 \rangle$ (a), $\langle P_4 \rangle$ (b), $\langle P_6 \rangle$ (c) and $\langle P_8 \rangle$ (d) measured by WAXS for RM734 (empty circles) and RM734-CN (filled circles) as a function of reduced temperature. The dashed line corresponds to the $N_S$-N transition in RM734, however as discussed in the text this transition is absent in RM734-CN.

## 6. References


1. O. Kratky, *Kolloid Z*, 1933, **64**, 0213-0222
2. P. Davidson, D. Petermann and A. M. Levelut, *J Phys Ii*, 1995, **5**, 113-131
3. M. T. Sims, L. C. Abbott, R. M. Richardson, J. W. Goodby and J. N. Moore, *Liq Cryst*, 2018, DOI: 10.1080/02678292.2018.1455227, 1-14
4. D. M. Agra-Kooijman, M. R. Fisch and S. Kumar, *Liq Cryst*, 2018, **45**, 680-686
5. R. J. Mandle, S. J. Cowling and J. W. Goodby, *Chemistry*, 2017, **23**, 14554-14562